Computers and Electronics in Agriculture 225 (2024) 109305

Contents lists available at ScienceDirect

Computers and Electronics in Agriculture

journal homepage: www.elsevier.com/locate/compag

Original papers

Optimized placement of sensor networks by machine learning for microclimate evaluation

Marco Zanchi [a,b,c,*], Stefano Zapperi [b,d,e], Caterina A.M. La Porta [a,b,f,g]

[a] Department of Environmental Science and Policy, University of Milan, via Celoria 10, 20133 Milano, Italy
[b] Center for Complexity and Biosystems, University of Milan, Via Celoria 16, 20133 Milano, Italy
[c] DNDG srl, Via Po, 57, 10124 Torino, Italy
[d] Department of Physics, University of Milan, Via Celoria 16, 20133 Milano, Italy
[e] CNR - Consiglio Nazionale delle Ricerche, Istituto di Chimica della Materia Condensata e di Tecnologie per l'Energia, Via R. Cozzi 53, 20125 Milano, Italy
[f] UOC Maxillo-Facial Surgery and Dentistry, Fondazione IRCCS Ca' Granda, Ospedale Maggiore Policlinico di Milano, via Francesco Sforza 28, 20122 Milan, Italy
[g] Innovation For Well-Being And Environment (CRC-I-WE), University of Milan, Via Celoria 10, 20133 Milano, Italy

ARTICLE INFO

Dataset link: https://github.com/dndg/MicroClimateOptSensorML

Keywords:
Precision agriculture
Microclimate
Artificial intelligence
Sensors placement
Local sensors measurements

ABSTRACT

Microclimate mapping and monitoring are of fundamental importance to manage natural resources and optimize agricultural procedures. Precision agriculture is based on the management of spatial–temporal microclimatic variation in fields monitored by IoT systems. Networks of microclimate sensors provide point-based measurements that can be used as input data for physical and artificial intelligence (AI) models to study variations of microclimatic conditions over several spatial and temporal scales. We propose and experimentally validate a computational framework based on AI algorithms to optimize and validate the placement of sensors networks according to local temperature variations within a study area located in the Lombardian foothills, Italy. The strategy involves a clustering procedure to extract spatial locations with a similar thermal behavior. An experimental validation has been then performed by deploying sensors in the optimized clusters to record temperature data. These data have been processed by a Nhits neural network trained to predict future temperature scenarios, to verify that predictions made inside each cluster are consistent and representative of a real temperature pattern. Our results indicate that the clustering optimization framework successfully identifies real temperature patterns within the study area.

1. Introduction

Precision agriculture is the ensamble of strategic approaches that integrate temporal, spatial, and individual data to enhance decision-making procedures in agricultural production. To effectively fulfill these objectives, the main processes impacting agricultural production must be understood and accurately monitored. Among these processes, microclimate stands out as a significant factor influencing agricultural outputs (Tanny, 2013; Schultze et al., 2021). Indeed, by accurately characterizing microclimate fluctuations (Comba et al., 2019), farmers can prevent the development of crop diseases and pests (Pangga et al., 2011), optimize irrigation strategies (Bwambale et al., 2022) and windbreaks placement procedures (Iwasaki et al., 2019).

Since microclimate is a complex, non-linear phenomenon (Chen et al., 1999) with meter scale fluctuations (Zellweger et al., 2019), monitoring systems able to collect data with high spatial and temporal resolutions must be employed. These systems can be identified by internet-of-things (IoT) technologies, which are recording systems able to collect and transmit data in real time (Farooq et al., 2020). By obtaining spatially and temporally precise measurements, farmers and agricultural researchers can gather data at specific points within the agricultural field (Anastasi et al., 2009). These data can be then exploited for predicting future scenarios with artificial intelligence and machine learning techniques (Kamilaris and Prenafeta-Boldú, 2018; Escamilla-García et al., 2020).

This approach offers reliable real-time predictions. However, it only provides information in locations where IoT technologies are deployed. Therefore, it is pivotal to ensure that the collected data accurately capture the full range of microclimate variations across the area of interest. Single climatic stations can be used to gather microclimate measurements over plains, where microclimatic variations do not diverge from macroclimatic ones (Oliver et al., 2018; Cicioğlu and Çalhan, 2021). Conversely, networks of multiple sensors should monitor microclimate over fields with complex topography (Sakthipriya, 2014; Khattab et al.,

* Corresponding author at: Department of Environmental Science and Policy, University of Milan, via Celoria 10, 20133 Milano, Italy.
E-mail address: marco.zanchi@unimi.it (M. Zanchi).

https://doi.org/10.1016/j.compag.2024.109305
Received 7 February 2024; Received in revised form 15 July 2024; Accepted 31 July 2024
Available online 7 August 2024

2016; Akhter and Sofi, 2022), where non-trivial and non-uniform microclimate variations emerge (Sai et al., 2016). Deploying a network of multiple sensors presents two conflicting challenges: increasing the number of sensors improves microclimate monitoring accuracy but it also raises costs for network establishment and maintenance. Therefore, opting for a uniformly distributed network of sensors, which may overlook microclimate variations, can result in significant expenses, particularly in large areas (Sai et al., 2016). The sensors should be instead strategically positioned according to the microclimate spatial variations. This approach enables the reconstruction of the entire spectrum of microclimate variations, ensuring an accurate monitoring at lower costs.

In the current state of the art, different strategies have been based on computational and mathematical methods to optimize sensors networks in open fields according to microclimate variations. Sai et al. (2016) have developed an algorithm named Optimized Algorithm of Sensor Node Deployment for Agricultural (OASNDFA), based on an optimized theory for the least required sensor nodes to monitor environmental variables of interest. The authors have validated their method in an orange orchard in China, identifying 5 sensors location with specific microclimatic variations. They have confirmed that the application of their method could enhance agricultural production in the field. Visalini et al. (2019) propose the Sensor Placement Algorithm with Range Constraints (SPARC), which optimally places sensors considering their range and according to microclimate. Based on convex relaxation techniques for NP-hard problems, the authors identify optimal locations that both maximize the accuracy of microclimate variations reconstruction and adhere to specific range constraints. The reconstruction of microclimate variations is achieved through the interpolation of sensor measurements and remote sensing data. The authors have tested their methods to reconstruct humidity variations reducing the number of needed sensors by 15%. Jia et al. (2021) have used the theory of compressed sensing (Eldar and Kutyniok, 2012) to optimize sensors placement according to soil moisture variations. The authors have initially proposed a grid of 64 sensors. The configuration has been optimized by selecting the minimum number of sensors which accurately reconstruct the soil moisture variations of the original grid. The authors optimized the sensor layout by reducing the number of sensors by one third while maintaining high accuracy in humidity reconstruction. The aforementioned mathematical methods and algorithms provide an accurate microclimate monitoring even in locations without sensors by reconstructing microclimate variations from the optimized sensor measurements. An alternative approach can be provided by machine learning clustering algorithms (Rodriguez et al., 2019).

Assuming that the microclimate variations are initially known across the entire agricultural field, machine learning clustering algorithms can automatically identify and group spatial locations with similar microclimate properties. As a result, it is possible to accurately describe microclimate variations within a cluster using measurements collected from a single sensor. Uyeh et al. (2022) have proposed this approach within the domain of indoor controlled agriculture. The authors have optimized a sensors layout within a protected cultivation system by employing a machine learning clustering algorithm, specifically the K-Means algorithm. This algorithm has been applied to temperature and humidity maps which represent the microclimatic variations across the entire protected cultivation area. The temperature and humidity maps have been generated from the interpolation of sensor measurements uniformly positioned across the cultivation area. The direct application of this method in an open field is challenging. Indeed, Uyeh et al. (2022) have generated temperature and humidity maps through interpolation techniques, which may be suitable for an indoor controlled environment operating at quasi-equilibrium. In contrast, open fields experience dynamic conditions far from equilibrium. Therefore, the application of interpolation techniques may overlook crucial microclimatic variations. Nonetheless, it is possible to reconstruct these complex microclimatic variations using algorithms which merge physical principles to data-driven methods (Kearney and Porter, 2017; Maclean et al., 2019). The optimized sensors layout should be then experimentally validated to assess if it accurately represents the real microclimate variation experienced by the area of interest. Sai et al. (2016), Visalini et al. (2019), Jia et al. (2021) and Uyeh et al. (2022) have performed experimental validations proving the robustness of their computational methods. However, predicting future microclimatic conditions using data from IoT sensors is a central focus in current deep learning applications for precision agriculture (Kamilaris and Prenafeta-Boldú, 2018). Therefore, it is crucial to verify that predictions made by optimized sensors also accurately represent real microclimate variations.

According to our knowledge, three distinct gaps occur in the current state of knowledge of sensors optimization for microclimate evaluation and monitoring of open agricultural fields:

- No research has been published yet on the optimization of sensors placement based on continuous microclimatic variations derived from physical laws.
- There has been no application of machine learning clustering methods, based on continuous microclimatic variations, to optimize the placement of sensor networks in open agricultural fields.
- No optimization method has been validated using predictions of future conditions made with deep learning models.

The present paper aims at filling these gaps by: (1) modeling with a physical model temperature variations at 2 m resolution in an open field with a complex terrain morphology; (2) proposing a computational framework based on a machine learning clustering algorithm to optimize a sensors layout according to the modeled temperature variations; (3) performing an innovative experimental validation, based on the Nhits deep learning algorithm (Neural Hierarchical Interpolation for Time Series Forecasting (Challu et al., 2023)) to predict the evolution of temperature and to verify that the optimized sensors layout is consistent with the future forecasting.

2. Materials and methods

2.1. Workflow design

In this paper we illustrate and experimentally validate a computational framework based on machine learning. This framework optimizes the deployment of a network of sensors according to the local temperature variations. The research has been conducted in a study area located in the Lombardian foothills in the province of Bergamo, Italy. The workflow design is proposed in Fig. 1.

2.1.1. Temperature variations

The temperature variations within the study area have been simulated at 2-m resolution, with a hourly frequency from November 12th, 2022, to June 22nd, 2023, exploiting a computational framework presented in the methods section. This procedure simulates continuous temperature variations at high resolution over the whole study area.

2.1.2. Sensors layout optimization

The simulated temperature variations have been processed by a machine learning clustering algorithm which groups spatial locations exhibiting similar thermal patterns. A clustering optimization procedure has been performed to optimally identify these regions. This procedure identifies the best clustering algorithm and the optimal number of clusters in which the study area should be divided. Once the optimal algorithm and number of clusters have been identified, the study area has been partitioned according to the relevant microclimate variations. A sensor can be then strategically placed within each optimal cluster providing representative temperature recordings for the

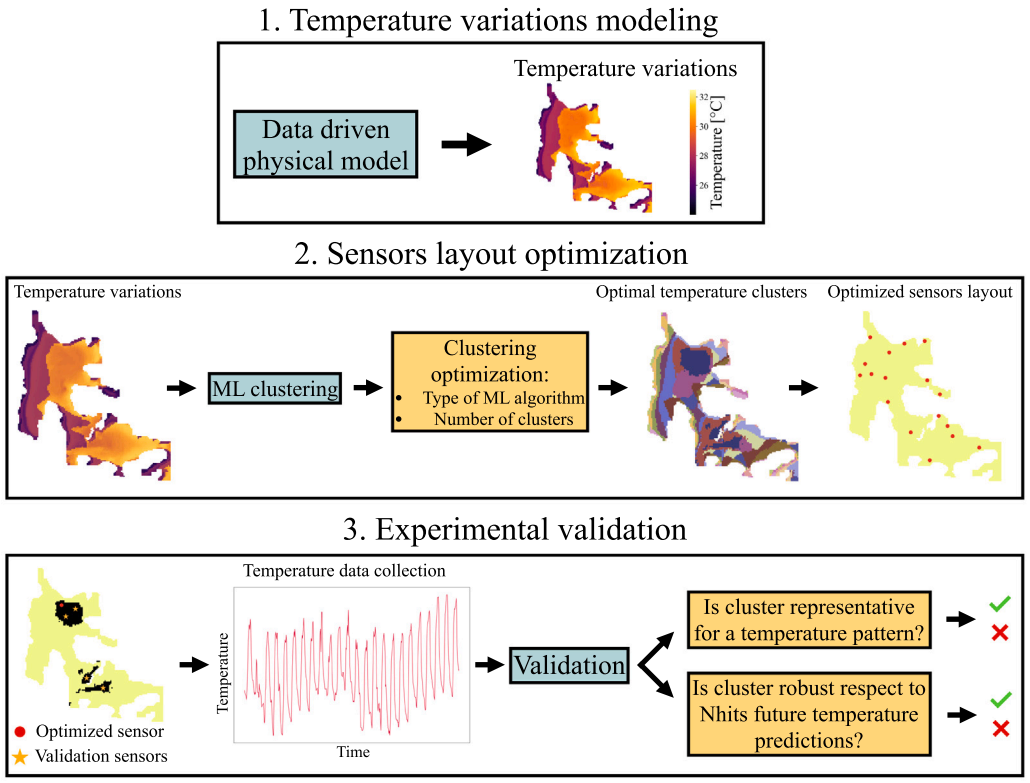

Fig. 1. Workflow design The figure describes the workflow design applied in this research. The pipeline is divided in three consecutive sections: the simulation of temperature variations from physical principles, the sensors layout optimization procedure and the experimental validation.

whole cluster. This sensor is defined as cluster center. This procedure leads to an optimized sensors layout designed according to the temperature variations of the study area. The workflow is summarized in the second step of Fig. 1.

2.1.3. Experimental validation

Since the temperature variations have been theoretically derived, an experimental validation procedure has been performed. This validation tests if the optimized clusters accurately represent and predict the real temperature variations. Four clusters have been selected for this validation and temperature data have been collected from different locations within them. The collected temperature data have been exploited to perform two different kind of validation. The first approach verifies that the optimized clusters and sensors are representative of the real temperature variations. This has been achieved by comparing the dispersion of temperature within the cluster with the overall temperature spread experienced by the study area. It has also been tested that the temperature pattern measured by the cluster center is more representative for the cluster points with respect to the points outside the cluster. The second approach demonstrates that future temperature predictions, made within the cluster by a deep learning algorithm, are consistent with respect to the ones made by the cluster center. In particular, a Nhits neural network has been trained to predict future temperature scenarios. The workflow is summarized in the third step of Fig. 1, for one of the four validation clusters.

2.2. Study area and monitoring sensors

The research has been conducted in the study area represented in Fig. 2B, located in province of Bergamo, Italy, in the Lombardy foothills (the location of the study area is shown in Fig. 2A). The study area is surrounded by woods and behind it there is a mountain of 700 m high. In the past, the study area has been used for vineyard crops, while it is currently exploited as mown meadows. The study area mainly faces east.

According to the Köppen and Geiger classification (Beck et al., 2018), the study area climate is humid subtropical (Cfa), with cold winters and warm and wet summers. Despite this, the Lombardy region shows significant climate differences with respect to the Köppen model due to proximity to large water basins and metropolitan areas, and local variability in elevation. Lombardy average annual rainfall is around 853 mm, with two minima in winter and summer and two maxima during the spring and autumn seasons. The annual average temperature is around 13.1 °C (55.5 °F).

20 sensors, based on MEMS technology, with hygrometers and thermometers, have been used to record temperature and relative humidity within the study area. The temperature measurement range provided by these devices spans from −20 to 60 °C, accurate to ±0.5 °C. While, for the relative humidity recordings, the sensors provide measurements within a 0 to 99% range, with an accuracy of ±5% RH. The devices transmit data exploiting Bluetooth Low Energy (BLE) connectivity, ensuring a smooth and efficient data collection process. Each sensor has been protected by a wood structure to cover it from the direct contact of rainfall. The locations of the 20 sensors have been indicated by red points in Fig. 2B.

The 20 sensors have collected data from July 23rd, 2023, to August 15th, 2023. Prior to utilizing the sensors in an outdoor environment, a calibration procedure has been conducted in controlled settings to minimize potential systematic calibration discrepancies, spanning from July 13th, 2023, to July 20th, 2023. Initially, a mean temperature and relative humidity profile have been determined by combining data from all sensors. Subsequently, the instantaneous deviation from this profile has been computed and averaged for each sensor. These values have been then designated as calibration parameters, to be subsequently subtracted from the field sensor measurements. Through the implementation of this calibration process, all systematic calibration errors have been rectified, improving the accuracy and reliability of temperature

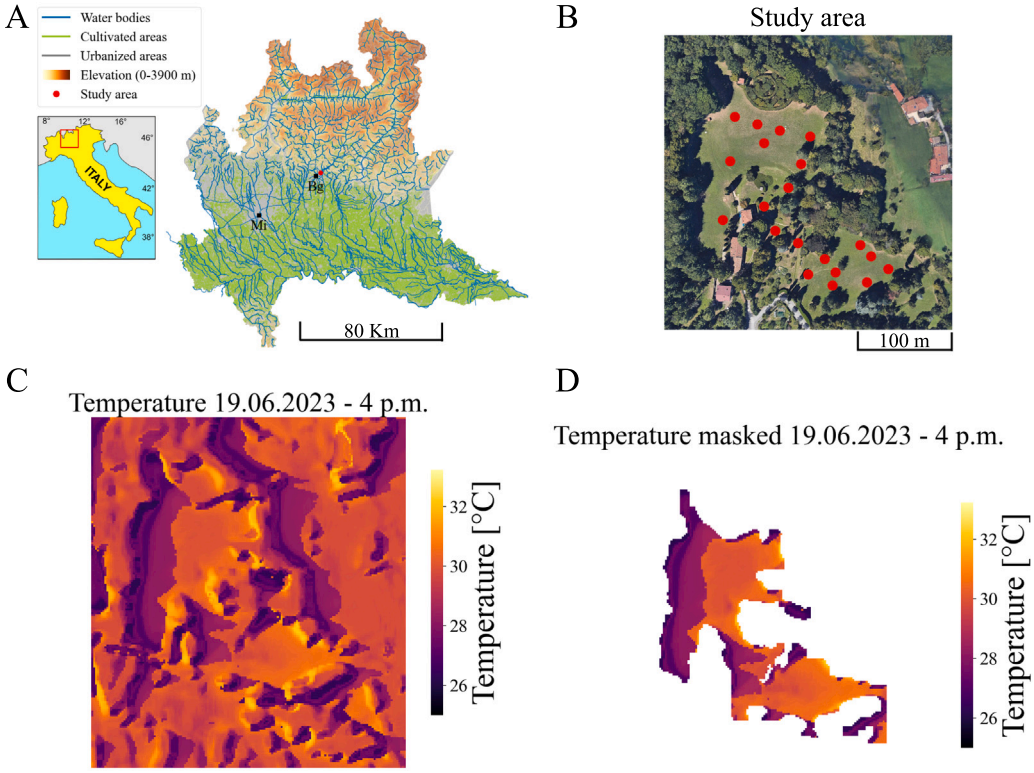

Fig. 2. Study area (A) The figure describes where the study area (red point) is located in Lombardy, Italy (Mi = Milan, Bg = Bergamo). The location of Lombardy is highlighted in the Italy representation on the left by the red square. The Lombardy figure has been taken and modified from Zanchi et al. (2022). (B) The figure displays the study area, which is located in the province of Bergamo in the Lombardian foothills, Italy (the center of the study area is located at 45°23′31″N 9°41′48″E). The image has been obtained from Google Earth Pro. The red points indicate the locations of the 20 sensors used in the experimental validation procedure. (C) The figure depicts the local temperature variation across the entire study area at June 19, 2023, at 4 p.m, predicted by a feed forward neural network. (D) The figure describes the local temperature variations across the vegetation free region of the study area at June 19th, 2023, at 4 p.m.

Table 1
Sensors data. The table describes the sensors data.

Sensors number	Recording period	Usage
25	November 12th, 2022, to June 22nd, 2023	Temperature reconstruction and Nhits transfer learning
20	July 23rd, 2023, to August 15th	Experimental validation procedures

and relative humidity measurements. In addition, the data collected by 25 sensors, presented in Zanchi et al. (2023), have been involved in the present research. The data have been exploited for the generation of the temperature maps at 2 m resolution and during the Nhits transfer learning procedure. These 25 sensors have collected temperature data from November 12th, 2022, to June 22nd, 2023. The two groups of sensors data have been described in Table 1.

2.3. Temperature variations of the study area

The temperature variations within the study area have been modeled at a resolution of 2 m, exploiting the computational framework described in Zanchi et al. (2023). It is summarized as follows. Initially, a microclimate model integrates climate data with the terrain morphology of the study area to determine 2-m-scale values of physical variables associated with the local temperature. Afterwards, a feed forward neural network has been trained, validated and tested using as input these downscaled variables to predict the local temperature at specific locations within the study area, where 25 sensors of the same type mentioned earlier have been uniformly deployed from November 12th, 2022, to June 22nd, 2023. The feed-forward neural network has been then utilized to perform a transfer learning procedure, predicting the local temperature across each location within the study area. This process generated a map, with a resolution of 2 m, illustrating the complete temperature variations across the entire study area. An example of a temperature map is represented in Fig. 2C for the June 19th, 2023 at 4 p.m. A total of 4488 temperature maps have been generated, covering the period from November 12th, 2022, to June 22nd, 2023, at hourly frequency, with some pauses in between due to sensors maintenance. A temperature map can be considered as a two-dimensional grid with a resolution of 2 m, where each grid location contains the corresponding temperature value.

Considering that the purpose of this research is to establish an optimized network of sensors for monitoring temperature fluctuations, it is reasonable that the sensors are not placed under the vegetation. To address this issue, a handcrafted vegetation map has been utilized, which specifically accounts for the non-vegetation-covered terrain. An illustration of a temperature map, where the vegetation is excluded, is depicted in Fig. 2D.

2.4. Machine learning clustering for sensors layout optimization

A clustering procedure has been applied on the temperature maps data in order to find the regions of the study area containing spatial locations which exhibit similar thermal patterns. The input dataset for the clustering procedure has been structured in the following way: the 4488 temperature maps have been aligned in the temporal domain, thus generating a time series reflecting the hourly temperature fluctuations on each grid location, spanning from November 12th, 2022, to June 22nd, 2023. A principal component analysis has been then performed on these time series, resulting in a vector of 50 principal components for each grid location within the study area. This number of principal

components accounts for the 90% of the overall variance. These principal components vectors can be then processed by a machine learning clustering algorithm to group together the grid locations exhibiting similar temperature variations. At this point two questions arise: which is the best clustering algorithm to apply? How many clusters should the study area be divided into?

A clustering optimization procedure has been performed to address these questions. The procedure has been divided in two steps: the choice of the optimal clustering algorithm and the search for the optimal number of clusters in which the study area should be divided into. We have conducted a comparison among three different clustering methods, the K-means algorithm, the agglomerative ward method, and the agglomerative complete method. For the determination of the optimal number of clusters, a systematic search has been conducted, evaluating the outcomes of each clustering algorithm for a number of clusters ranging from 2 to 25.

In the clustering optimization procedure, the outcome generated by each clustering algorithm, tested with different number of clusters, have been evaluated using two metrics: the cluster mean absolute error concerning the cluster center, and the silhouette score. The optimal algorithm which divides the study area in the optimal number of clusters is the one which minimizes the cluster mean absolute error concerning the cluster center and maximizes the silhouette score. Therefore, the clustering optimization procedure concerns the optimization of two-objectives.

The clustering procedures have been performed through the scikit Python library.

2.4.1. K-means clustering algorithm

The K-means algorithm has been exploited to find clusters of spatial points which have similar trends in their temperature variation. The K-means algorithm is an unsupervised clustering technique that aims at partitioning N observations, X, represented by vectors of numbers (in the present case by the PCA vector of the temperature time series) into K clusters, C, containing the observations with a similar mean (Hartigan and Wong, 1979). The clustering procedure follows an optimization strategy defined as:

$$\sum_{i=0}^{N} \underset{\mu_j \in C}{min} (\|x_i - \mu_j\|) \tag{1}$$

where μ_j are the mean of the observations X in a cluster C. The algorithm requires as input the number of clusters K. This procedure has been reproduced for a number of clusters spanning from 2 to 25.

2.4.2. Agglomerative clustering

Agglomerative clustering is a hierarchical clustering algorithm which creates clusters by a bottom up procedure. At the start, each observation is placed in its own cluster and then clusters are successively merged together according to the minimization of a certain metric (the two clusters that minimize the metric are merged in a new cluster). The choice of the metric defines the kind of agglomerative clustering. In the present research the ward and the complete agglomerative clustering methods have been exploited.

The ward agglomerative clustering minimizes the sum of squared differences within all clusters (Ward, 1963). Given a cluster A and a cluster B the ward metric is defined as:

$$d_{ward} = \sum_{x \in A \cup B} \|x - \mu_{A \cup B}\|^2 - \sum_{x \in A} \|x - \mu_A\|^2 - \sum_{x \in B} \|x - \mu_B\|^2 \tag{2}$$

The complete linkage minimizes the maximum distance between observations of pairs of clusters. Given a cluster A and a cluster B the complete metric is defined as:

$$d_{complete} = \max_{a \in A, b \in B} |a - b| \tag{3}$$

2.4.3. Clustering optimization metrics

Two metrics have been defined to determine the most suitable clustering method and the appropriate number of clusters. The first metric involves the mean absolute error with respect to the cluster center. The second metric employed is the silhouette score. The first metric is defined as follows. Given a partition of the grid locations of the study area in C clusters, for each cluster C_i a location j is chosen as candidate for being the center of the cluster and the mean absolute value between its feature vector Φ_j and the rest of the locations k feature vector Φ_k is computed. The location j_c which obtains the minimum of the mean absolute error is considered the cluster center. The error is computed and averaged for each cluster C_i :

$$MAE_{center} = \frac{\sum_{i=1}^{C} \min_{j \in C_i} \left\langle |\Phi_k - \Phi_j| \right\rangle_{k \neq j, k \in C}}{C} \tag{4}$$

where the symbol $\langle \cdot \rangle_k$ means an average over the index k.

The silhouette score (Rousseeuw, 1987) measures how much an object is similar to its own cluster compared to the other clusters. The silhouette score ranges from 1 to −1. Positive values towards 1 mean that the object is very similar to the other cluster members, while negative values towards −1 mean that it is poorly matched. The silhouette score s_i for an object i belonging to the cluster I is defined as:

$$s_i = \frac{b_i - a_i}{\max(a_i, b_i)} \tag{5}$$

where

$$a_i = \langle d(i,j) \rangle_{j \in I, j \neq i} \tag{6}$$

$$b_i = \min_{J \neq I} \langle d(i,j) \rangle_{j \in J} \tag{7}$$

and $d(i,j)$ is the euclidean distance

$$d(i,j) = \|i - j\|^2 \tag{8}$$

In the present paper the silhouette score for evaluating the optimal number of clusters and clustering methods is computed averaging the silhouette score over all the grid locations of the study area:

$$S = \langle s_i \rangle_{study area} \tag{9}$$

2.5. Experimental validation procedure

An experimental validation has been performed to assess whether the optimized sensors layout accurately represents the actual and future microclimate conditions of the study area. This validation is motivated by the fact that the clusters have been generated from theoretical modeled temperature maps.

Four clusters have been selected for the experimental validation procedure. A central point has been defined within each cluster and a sensor has been placed at this point. The temperature pattern recorded by this sensor should represent the characteristic temperature pattern described by the whole cluster. In addition, four other sensors have been positioned at different locations for each validation cluster. Therefore, for each validation cluster a total of 5 sensors have been positioned (for a total of 20 sensors). These sensors have collected temperature data from July 23rd, 2023, to August 15th, 2023. The data have been then analyzed to address two different validation tasks. The first task aims at verifying that the optimized clusters represent a characteristic temperature pattern of the study area and that the optimized sensors record representative temperature variations of their clusters. The second task validates that future temperature predictions made by a Nhits neural network, using as input the optimized sensors data, are representative for the future temperature variations experienced in the optimized clusters.

2.5.1. Validation of real temperature representation

At first, for each sensor i, the hourly temperature time series has been normalized by the average hourly time series over all the 20 sensors, S, (5 sensors for each cluster) in order to remove scale effects:

$$T^i_{norm} = \frac{T^i - \left\langle T^j \right\rangle_{j\in S}}{\langle T^j \rangle_{j\in S}} \tag{10}$$

The normalized temperature time series have been analyzed with two distinct approaches. The first approach compares the dispersion of temperature readings within the cluster with the overall temperature spread recorded by all 20 sensors deployed across the study area. This approach involves calculating the standard deviation of the mean for each hour across the cluster temperature time series and subsequently comparing it with the standard deviation calculated across all the measurements from the 20 sensors. The two curves have been then compared with a Mann–Whitney U statistical test (Mann and Whitney, 1947) to test if the cluster spread curves is statistically lower than the spread curve obtained with the data gathered outside the cluster.

The second approach computes, for each cluster, the distribution of absolute differences among the temperature readings of the cluster central sensor and the other sensors within the same cluster. This is then compared with the distribution of absolute differences between the temperature readings of the cluster central sensor and the sensors that are not located in the cluster. The comparison has been performed through a Mann–Whitney U statistical test, to test if the distribution of the absolute differences of the temperature measured inside the cluster is statistically less than the one measured outside the cluster.

A removal strategy has been implemented for each cluster to address potential dependencies on individual sensor behaviors in the validation results. This strategy ensures the robustness of validation results against individual behaviors within clusters. The removal procedure is based on a validation process with respect to the cluster center while excluding one cluster sensor at a time (this is repeated for each sensor in the cluster). The Mann–Whitney U statistical test results are specifically used as a measure to evaluate the impact of individual sensor behaviors.

2.5.2. Validation of future conditions forecasting

Since the optimized sensors should be exploited for monitoring microclimate conditions and predicting future scenarios, it is important that the future temperature predictions made by different locations inside a cluster are consistent with the predictions made at the cluster center. A validation strategy for future conditions forecasting has been performed on the microclimate data measured by the 20 sensors from July 23rd, 2023, to August 15th, 2023. A Nhits has been trained to forecast the temperature evolution in the next 24 h given temperature and humidity data from the past 72 h. The details regarding the Nhits architecture and training are described in the next section. For each of the four validation clusters, the distribution of the absolute differences between the temperature values predicted from the data measured by the cluster center sensor and the temperature prediction obtained from the data measured by the sensors located inside the cluster has been computed. This distribution has been then compared to the one obtained computing the absolute differences between the temperature values predicted from the data measured by the cluster center sensor and the temperature prediction obtained from the data measured by the sensors located outside the cluster. Since the Nhits produces probabilistic temperature predictions, the median of the predicted temperature quantile distribution has been used to compute the absolute differences. The comparison of the two distribution has been performed through a Mann–Whitney U statistical test to test if the distribution of the absolute differences of the temperature measured inside the cluster is statistically less than the one measure outside the cluster.

2.5.3. Nhits

Nhits (Neural Hierarchical Interpolation for Time Series Forecasting (Challu et al., 2023)) is a neural network specialized in time series long-horizon forecasting by learning how to apply a multi-rate sampling of the input signal and a multi-scale synthesis of the forecast. The input signal is decomposed into its fundamental frequency modes which are then combined to generate long-horizon prediction results. This hierarchical approach to forecasting significantly reduces computational requirements and enhances forecasting accuracy. The Nhits architecture is organized into S stacks, each specializing in learning a distinct characteristic of the data. Each stack comprises a set of B blocks. Within each block, there is a multilayer perceptron that generates forecast outputs based on its features and a backcast used to eliminate the component related to its features from the input signal, which is then utilized for the subsequent block. This approach has surpassed various modern transformer-based architectures on different baseline datasets. For additional technical and numerical details, please refer to Challu et al. (2023).

In the current study, an Nhits architecture has been used for generating long-horizon probabilistic predictions of temperature. With a given hourly time series of temperature, the input comprises the temperature data from the past 72 h. The prediction involves forecasting the quantile distribution of the temperature data for the next 24 h. In addition to the input temperature data, a time series of relative humidity has been incorporated to expand the input variance space. The prediction involves the estimate of a probabilistic value for the temperature at each hour (for the next 24 h) based on the temperature quantile distribution learned during the training procedure using a quantile loss (Wen et al., 2017):

$$Q = \sum_t \sum_q \sum_{h=1}^{24} L_q(y_{t+h}, y^p_{t+h}) \tag{11}$$

where

$$L_q(y, y^p) = q(y - y^p)_+ + (1-q)(y^p - y)_+ \tag{12}$$

where t is the start of the forecasting horizon, q is the quantile and h is the hour in the forecasting horizon. The $(x)_+$ operation for a generic number x stays for $\max(0, x)$.

The Nhits model has been trained, validated, and tested using temperature and relative humidity data gathered from an ARPA meteorological station situated near the study area, covering the period from 2018 to 2022. The training set comprises data from 2018 to 2020, the validation set consists of data collected in 2021, and the test set encompasses data collected throughout 2022.

The optimization process in this study employs the Adam optimizer (Kingma and Ba, 2014), an advanced gradient descent optimization algorithm. Adam, short for Adaptive Moment Estimation, is renowned for its efficacy in optimizing neural networks. With Adam, the adjustment of the network's weights occurs iteratively, utilizing both the first and second moments of the gradients. This adaptive approach enables the dynamic updating of the learning rate for each weight parameter.

The hyperparameters for Nhits have been chosen following a grid search optimization process, leading to the selection of 6 stacks, each containing 2 blocks. Within each block, the multilayer perceptron comprises 2 layers, each with 128 neurons. The specific configuration of Nhits hyperparameters represents the set of values that minimized the loss function on the validation set during the grid search optimization process. The entire set of hyperparameters is shown in the supplementary materials.

The optimized Nhits has been trained for 1000 epochs on the training set, with a patience of 100 epochs on the validation set. Then the Nhits has been evaluated on the test set. Before delving into the evaluation metric used to assess the prediction capability of the trained Nhits, it is beneficial to recap how the neural network formulates

predictions. With the input consisting of data from the preceding 72 h of temperature and relative humidity, the Nhits forecasts a temperature value for each of the subsequent 24 h based on the quantile distribution learned during the training phase. In this study, a set of 17 quantiles has been employed, including 8 quantile bands and 0.5 as the central quantile. The quantiles bands are $(0.01, 0.99)$, $(0.05, 0.95)$, $(0.10, 0.90)$, $(0.15, 0.85)$, $(0.20, 0.80)$, $(0.25, 0.75)$, $(0.30, 0.70)$, $(0.40, 0.60)$. By repeating the predicting procedure on a fixed input, it is possible to reconstruct an estimation of the quantile distribution for the temperature for the next 24 h (it is possible to derive the temporal evolution of the quantiles for the next 24 h). Prediction examples are shown in Fig. 7A,C. The quality of the probabilistic prediction has been evaluated on the test set through the mean absolute error (MAE) of the mean and the median of the sampled distribution (with 1000 predicted samples):

$$MAE_{mean}(y, y^p) = \frac{\sum_{i=1}^{N} |\langle y_i^p \rangle - y_i|}{N} \tag{13}$$

where $\langle y_i^p \rangle$ is the mean of the sampled prediction distribution (with 1000 prediction samples).

$$MAE_{median}(y, y^p) = \frac{\sum_{i=1}^{N} |\tilde{y}_i^p - y_i|}{N} \tag{14}$$

where $\tilde{y}$ is the median of the sampled prediction distribution (with 1000 prediction samples).

A validity measure has been exploited to evaluate the reliability of the quantile prediction. The validity is defined as follows. For a given quantile band (a, b), a prediction sampled from a quantile distribution should fall within this band in the $(b - a)\%$ of cases. By repeating the temperature prediction for each input 1000 times, an estimate of the predicted temperature quantile distribution for the next 24 h has been built. It is then possible to count how many times the real temperature falls within each quantile band defined by the estimated distribution over the 24 h. The validity measure for a quantile band (a, b) can be defined as the average of this counts over all the predictions:

$$Validity(a, b) = \frac{\sum_{i=1}^{N} \sum_{h=1}^{24} v(y_i(h), a, b)}{N} \tag{15}$$

where $y_i(h)$ is the real temperature scenario i at hour h and $v(y_i(h), a, b)$ is 1 if $y_i(h)$ belongs to the quantile band (a, b) and 0 in the opposite case. If the $Validity(a, b)$ value is near to $(b - a)\%$ the probabilistic predictions works. The validity measure helps assessing whether Nhits can produce a reliable probabilistic forecast.

After training, validating, and testing the Nhits on the data collected by the ARPA station near the study area, a transfer learning procedure has been implemented to transfer the Nhits skills on data measured by the sensors deployed over the study area. The transfer learning process involves reusing (without training it again) the Nhits model trained on the ARPA data for the sensor data from November 12th, 2022 to August 15th, 2023 (with some pauses in between), assuming that the temperature patterns observed by the ARPA station are comparable to those measured by the sensors. The metrics used during the test have been recalculated for the transfer learning procedure to assess the quality of transfer learnt predictions on the sensors data. The choice of using the data from an ARPA station is motivated by the need of a large amount of data to effectively and properly train, validate and test the Nhits. The Nhits architecture has been built, trained and tested using the Darts Python library (Herzen et al., 2022).

3. Results and discussion

This section analyzes and discusses the results of the current research. It begins by outlying the results of the clustering optimization procedure, followed by an overview of the resulting optimized clusters. Then, the results obtained during the two phases of the experimental validation have been described.

3.1. Clustering optimization results

A clustering procedure is applied to the temperature maps to identify spatial regions within the study area that show similar temperature variations over time. The clustering optimization procedure compares three different clustering methods and finds the optimal number of clusters into which partition the study area. In order to find the optimal number of clusters and the optimal clustering method, two metrics have been exploited: the mean absolute error with respect to the cluster center, defined in Eq. (4), and the silhouette score, defined in Eq. (9). These two metrics have been computed for different numbers of clusters and for different clustering methods. The results are shown in Fig. 3. Fig. 3A compares the results for the mean absolute error with respect to the cluster center obtained for a number of clusters ranging from 2 to 25 and for three different clustering algorithms (K-means, agglomerative ward and agglomerative complete). Fig. 3B shows the silhouette score computed for a number of clusters ranging from 2 to 25 and for three different clustering algorithms (K-means, agglomerative ward and agglomerative complete). The K-means algorithm shows better performances with a lower MAE_{center} error and a higher silhouette score with respect to the agglomerative clustering methods. This result is confirmed by the work of Uyeh et al. (2022), where a K-means clustering algorithm has been chosen to cluster temperature and humidity time series.

As shown in Fig. 3A, the error with respect to the cluster center continuously decreases until reaching 17 clusters. From 17 clusters onwards the decline is smoother and not significant. Fig. 3B shows the silhouette score remaining relatively steady from 10 clusters onwards. These results suggest that there are no significant differences in the number of clusters between 17 and 25. Given that more clusters require deploying additional sensors, which increases network costs, selecting 17 clusters as the optimal number appears to be a reasonable choice. Given the relatively small study area and the relatively small cost of temperature sensors, the implementation of a network of 17 sensors should not incur significantly higher costs compared to a network of 25 sensors. However, the primary objective of the paper has been to establish a general framework applicable to areas of varying dimensions and capable of clustering any physical variables. In scenarios where the area of interest is large and requires a high number of monitoring sensors, the reduction achieved through the clustering optimization procedure becomes especially crucial for cost-effectiveness. Moreover, in instances where high-cost sensors are necessary, the clustering optimization procedure can significantly mitigate the overall cost of the sensors network. We have collected the clustering results for all alternative numbers of clusters in the supplementary materials, providing a more comprehensive comparison of the clustering outcomes (supplementary Figure 5, 6, 7).

The K-means algorithm has been applied to the temperature maps data partitioning the study area in 17 clusters, as represented in Fig. 3C. A collection of the single cluster maps is provided in the supplementary material (from supplementary Figure 1 to 4). Inside each cluster, a central point has been identified as the cluster center and a sensor has been placed there. The optimized layout of 17 sensors is represented in Fig. 3D. Certain clusters exhibit compactness and accurately capture characteristic temperature variations, whereas others are less easily interpretable. Fragmented clusters emerge near to the edges of the study area. This phenomenon can be attributed to the increased influence of vegetation in these areas, which complicates temperature modeling and results in high temperature variability. Another explanation for these less interpretable clusters could be attributed to the challenge that the clustering procedure encounters in distinguishing discrete differences among continuous objects, such as the temperature time series. This challenge is particularly evident from the silhouette coefficient values depicted in Fig. 3B, which are relatively low. Ideally the silhouette coefficient should approach 1 for a perfect clustering. It is worth noting that similar magnitude values for silhouette coefficients were

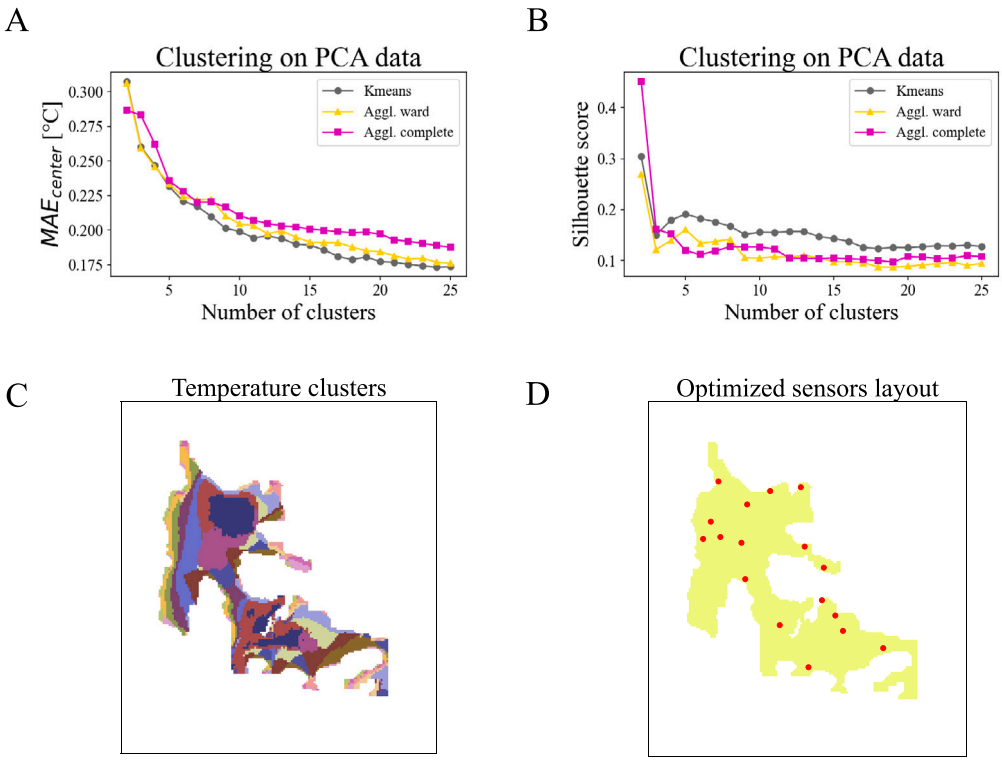

Fig. 3. Clustering procedure (A) The figure describes the MAE_{center} metric defined in (4), represented on the Y axis, for different number of clusters, described on the X axis, and for the three different clustering methods (described in the legend: Kmeans stays for the K-means clustering algorithm, Agg. ward stays for the agglomerative ward clustering algorithm and Agg. complete stays for the agglomerative complete clustering algorithm). (B) The figure describes the silhouette score defined in (9), represented on the Y axis, for different number of clusters, described on the X axis, and for the three different clustering methods. (C) The figure describes the study area divided in 17 clusters by the K-means algorithm. (D) The figure describes the optimized sensors layout with the 17 optimized sensors represented by red dots.

also found in Uyeh et al. (2022) for optimal clusters. The introduction of temperature variations derived from physical principles introduces additional variability, particularly in areas where multiple environmental factors contribute to complex temperature patterns. These patterns can be challenging to group together into spatial clusters, especially when compared to cases of simple interpolation, which tend to smooth out sudden variations. Hence, from a cost-optimization perspective, it is reasonable to adjust the optimized sensors layout by removing those that are situated in less interpretable locations. Nonetheless, the primary objective of this paper was to demonstrate that clustering methods can effectively generate clusters of temperature variations corresponding to real physical scenarios.

3.2. Analysis of clusters used in experimental validation

Out of the 17 clusters generated by the K-means algorithm, 4 clusters have been selected for the experimental validation due to their apparent physical and interpretable meaning. They are respectively identified as cluster 0, cluster 2, cluster 6 and cluster 10. Cluster 0 is depicted in Fig. 4A. It characterizes a large basin with a gradually declining slope, accompanied by two additional separate, smaller basins. Cluster 2 is displayed in Fig. 4B, outlining a significant area parallel to the vegetation in the western part of the study area. This cluster is expected to include grid locations that are shaded in the afternoon as the sun descends behind the hill situated at the western rear of the study area. The cluster also includes other smaller and not compact regions parallel to the big one. Cluster 6 is illustrated in Fig. 4C, characterizing regions with decreasing slopes oriented towards the east. Cluster 10 is shown in Fig. 4D, representing areas shaded by vegetation in the morning when the sun is positioned in the lower right corner of the study area. The selection of these clusters is additionally bolstered by the fact that they consistently emerge when applying the clustering procedure, even with varying numbers of clusters different from 17. This consistency indicates that they truly represent robust representations of temperature patterns delineated by the physical model.

The clusters can consist of non-continuous structures representing the same microclimate condition across various regions of the study area, indicating a form of non-local behavior. This underlines the necessity of employing sensor optimization strategies for microclimate assessments. Utilizing a network of sensors uniformly distributed across the area of interest would introduce redundancies in measurements, leading to increased costs without necessarily providing additional valuable information. Therefore, optimizing sensor placement based on clustering analysis can lead to more efficient and cost-effective data collection approaches for microclimate evaluations.

For each cluster, a center has been identified and indicated in Fig. 4 by a red point. This center is the most representative point of the temperature variations described by the cluster. In practice, placing a sensor to monitor the microclimate at this point serves as a proxy for the temperature across all other points within the cluster. This approach facilitates an accurate reconstruction of the temperature distribution across the study area. We have introduced 4 other locations within each cluster, represented in Fig. 4 by the yellow stars. We have placed a sensor in each of these locations to collect the data used for the experimental validation. These points have been selected to monitor specific area of the clusters. Priority has been given to placing sensors in non-continuous area, as these areas may be influenced by non-local effects generated by the theoretical modeling, which may not reflect a real temperature pattern.

3.3. Experimental validation: are optimized clusters representative of real temperature variations?

An experimental validation of the sensors layout optimization has been performed to determine if the clusters obtained from theoretical

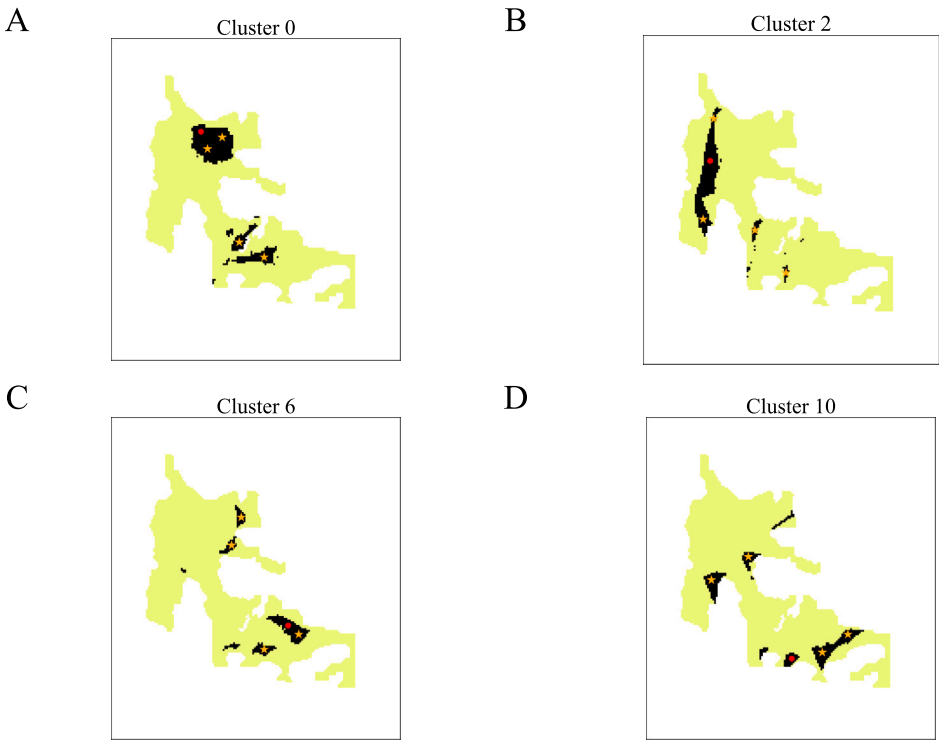

Fig. 4. Clusters maps The figures describe the four validation clusters involved in the validation procedures. The red point is the cluster center and the stars represent the other 4 sensors deployed in the cluster.

temperature maps effectively represent the real microclimate conditions of the study area. To summarize, for each validation cluster, five sensors have been deployed: one at the cluster center and the remaining four at other cluster locations. Then the sensors have recorded the temperature from July 23rd, 2023, to August 15th, 2023. This data have been then analyzed with two different approaches as described in the Method section. The initial approach aims to assess whether the temperature spread within the cluster is lower than the overall spread within the study area. After normalizing the hourly temperature, the standard deviation has been computed for the cluster time series for each hour. The same procedure has been applied to the temperature time series of all the sensors. If the cluster shows a narrower spread than the overall microclimate conditions, the cluster curve is expected to lie beneath that of the overall data. In order to assess this in a robust statistical way a Mann–Whitney U statistical test has been performed on the two data distribution to assess if the cluster temperature spread is statistically less than the spread outside the cluster. The two spread curves have been plotted for each cluster in Fig. 5. As shown in Fig. 5A, B, the two curves exhibit a comparable spread, indicating that cluster 0 and 2 are not particularly representative of the actual microclimate conditions, as confirmed by the Mann–Whitney U statistical test (Pvalue higher than 0.05). Instead, Fig. 5C, D illustrate that the cluster spread curve is lower than the one representing the overall temperature spread, indicating that clusters 6 and 10 are representative of the actual microclimate conditions, as also corroborated by the Mann–Whitney U statistical test (Pvalue less than 0.05).

The second validation approach aims at comparing, for each cluster, the distribution of absolute differences between the temperature readings of the cluster central sensor and those of the other sensors within the same cluster with the distribution derived from comparing the central measurements with the data measured by sensors located outside the cluster. Fig. 6 shows the two distributions for each cluster. A Mann–Whitney U statistical test has been applied to test if the distribution of the absolute differences of the temperature measured inside the cluster is statistically less than the one measure outside the cluster. The results are consistent with the findings of the analysis of the temperature spread inside and outside the cluster. Fig. 6A and B show that the two distributions have a similar shape, meaning that the clusters 0 and 2 are not very representative of the actual microclimate conditions. This is also confirmed by the Mann–Whitney U statistical test which in both cases shows a Pvalue greater than 0.05 for the null hypothesis that the distribution of the temperature differences inside the cluster is not statistically less than the one outside the cluster. Fig. 6D and C compare the distribution of the cluster temperature difference for clusters 6 and 10 to the one obtained outside the clusters. For both clusters, the first distribution shows a higher peak for small values of absolute errors, while the second has larger tails for high values of absolute error. This behavior is also confirmed in both cases by the Whitney U statistical test which shows a Pvalue less than 0.05. Therefore, it is possible to reject the null hypothesis that the distribution of the temperature differences inside the cluster is not statistically less than the one outside the cluster.

To address potential dependencies of the clustering validation results on individual sensor behaviors, the removal strategy described in the Methods section has been performed for each cluster. For each cluster, a sensor at time is removed and the two validation approaches are performed. If the results are the same as in the normal case (the case with all the four sensors), it means that no individual sensors can influence the clustering validation results. From this analysis, it appears that the validation results for clusters 2, 6 and 10 are robust towards single sensor behaviors. One sensor in cluster 0 (the third star from top to bottom in Fig. 4A) influences the clustering validation results. Removing this sensor makes the Mann–Whitney U statistical test Pvalue lower than 0.05 for both validation approaches. This finding may be explained by the location of that particular sensor, which is positioned near the vegetation border. This fact may influence the microclimatic behavior in this particular location so that the theoretical temperature maps do not describe the real temperature variations properly.

The validation analysis reveals that cluster 0 is not totally representative of a characteristic temperature variation, since there is an area which behaves differently with respect to other cluster points. Cluster 2 appears to inadequately represent a characteristic temperature pattern, although it seems to capture a pattern related to the shadow

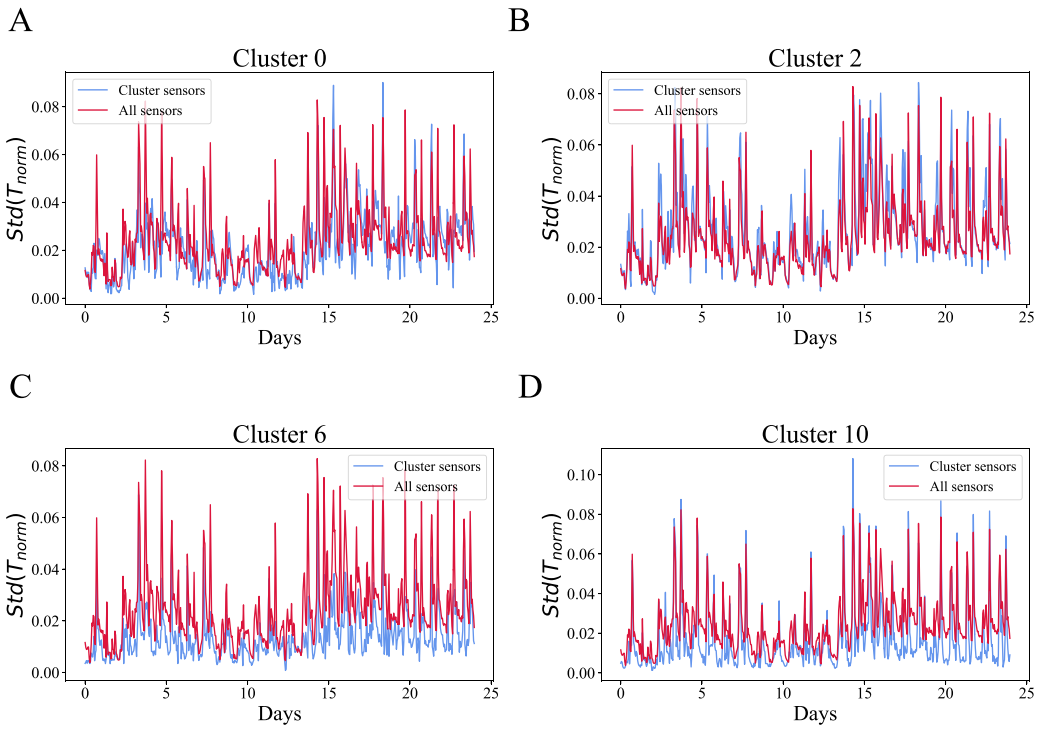

Fig. 5. Clustering validation: temperature dispersion. The figures describe the hourly temporal evolution of the normalized temperature standard deviation measured inside the cluster (in red) and the normalized temperature standard deviation measured by all 20 sensors (in blue). The X-axis represents the time in hours, while the Y-axis represents the normalized temperature standard deviation. The figures A, B, C and D describe respectively the data for the validation clusters 0,2,6 and 10.

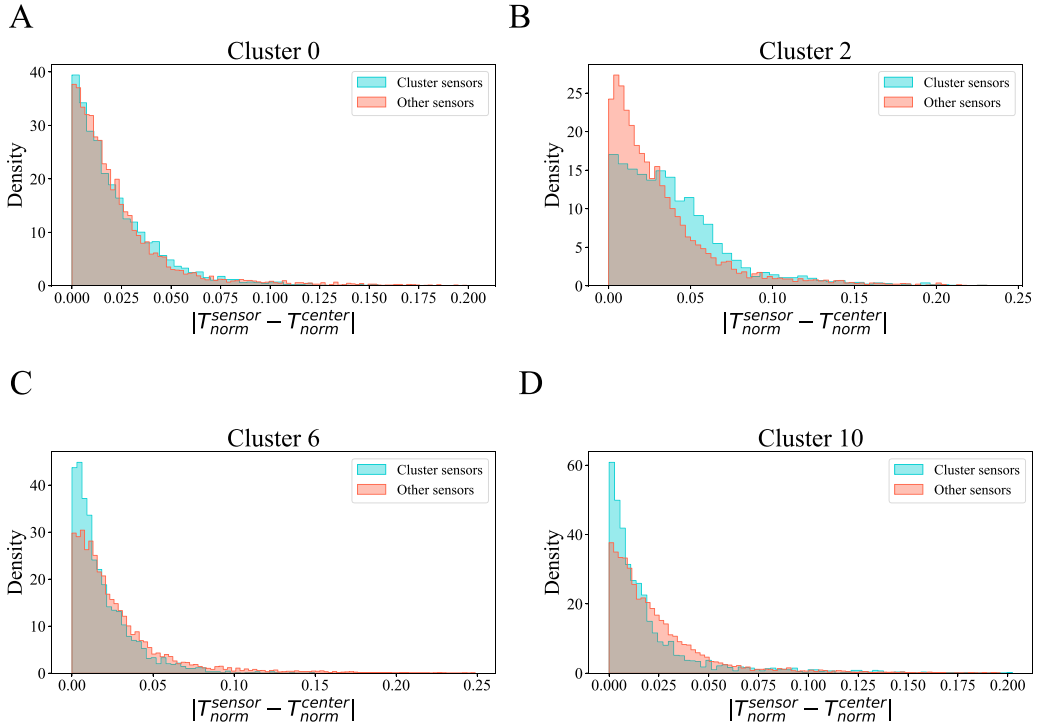

Fig. 6. Clustering validation: absolute temperature differences from the cluster center. The figures describe the distributions of the normalized temperature absolute difference between the cluster center and the cluster elements (in light blue) and the distribution of the normalized temperature absolute difference between the center of cluster and all the other elements not in cluster (in red). The figures A, B, C and D describe respectively the data for the validation clusters 0,2,6 and 10.

cast by the vegetation. Fig. 3 also shows other structures similar and parallel to cluster 2. These parallel clusters may represent the leading edges of shadows cast by vegetation moving from left to right across the study area, as the afternoon progresses. An explanation for the failure in the validation procedure of cluster 2, may reside in the error made by the physical modeling in replicating the perfect timing of the shadows movements. It is also noteworthy that the validation was conducted in August, while the temperature maps depict variations

Table 2
Test results for validity measure.

Quantile bands	Validity measure
(0.01, 0.99)	0.975
(0.05, 0.95)	0.905
(0.10, 0.90)	0.802
(0.15, 0.85)	0.704
(0.20, 0.80)	0.603
(0.25, 0.75)	0.500
(0.30, 0.70)	0.400
(0.40, 0.60)	0.198

Validity measure results on the test set for all the quantile bands.

Table 3
Transfer learning results for validity measure.

Quantile bands	Validity measure
(0.01, 0.99)	0.960
(0.05, 0.95)	0.894
(0.10, 0.90)	0.808
(0.15, 0.85)	0.719
(0.20, 0.80)	0.626
(0.25, 0.75)	0.528
(0.30, 0.70)	0.426
(0.40, 0.60)	0.213

Validity measure results on the transfer learning data for all the quantile bands.

occurring from November to June. During these periods, the solar elevation angle of the sun varies, leading to different movements in the progression of shadows. Cluster 6 and cluster 10 are representative of an actual partition of microclimate on the study area. In these two cases the model seems to perform correctly in representing a real temperature variations showing non local behaviors. Therefore, it has been experimentally tested that it is possible to deploy a sensor in the cluster center and represent the whole cluster temperature variation with measurements gathered by this sensor.

The observation that certain clusters fail to accurately represent real temperature variations underlines the challenges inherent in modeling and clustering microclimate patterns over open fields, particularly when compared to the use of interpolation methods or in controlled indoor environments. Despite some failures, the validation of clusters 6 and 10 confirms the existence of non-local microclimate patterns. This is significant because the application of spatial interpolation methods to address microclimate variations over open fields can result in misleading representations. Interpolation relies on spatial locality, which may produce inconsistent results when dealing with non-local microclimate structures.

3.4. Experimental validation: future conditions forecasting with Nhits

The measurements obtained from the clusters centers can be used to train neural networks capable of predicting future scenarios, offering valuable information for risk management strategies. It is crucial that future predictions based on the cluster center data remain consistent with the predictions that can potentially be derived from other cluster points. Thus, a validation strategies for future conditions has been performed as described in the Methods section. A Nhits architecture has been trained for a probabilistic forecast horizon prediction, employing the microclimate data for the preceding 72 h as inputs and forecasting the subsequent 24 h as output. The neural network has been trained, validated and tested on the temperature and relative humidity data collected from an ARPA meteorological station located nearby to the study area from 2018 to 2022. An example of a prediction performed by the Nhits is shown in 7A. In order to test the Nhits predictive capability the median and mean absolute error of the prediction have been computed for the test set and plotted against the baseline error (which is the error obtained using as prediction the last 24 h from the input data) in Fig. 7B. Notice that the distributions for the predictions contain lower errors with respect to the baseline as confirmed by the Mann–Whitney U statistical test Pvalue which is less than 0.05. In addition, the validity measure has been computed for all the quantile bands (Table 2). Note that all the validity measures are reasonably near to the quantile bands width suggesting that the Nhits is providing reliable predictions.

A transfer learning procedure has been applied in order to test if the Nhits trained on the data collected by the ARPA station located in the proximity of the study area is capable of making reliable predictions on data collected by the sensors. An example of a prediction over the data collected by sensor 1 is provided in Fig. 7C. The transfer learning results of Nhits prediction capability are shown in Fig. 7D where the distribution of the median absolute prediction error defined in Eq. (14) is compared to the baseline error distribution. For the transfer learning procedure the distribution of the median absolute prediction error contains lower errors with respect to the baseline as confirmed by the Mann–Whitney U statistical test Pvalue which is less than 0.05. Also in this case the median prediction is significantly lower than the baseline as proved by the statistical test and in 7D.

The validity analysis has been performed in Table 3. Also in this case, all the validity measures are reasonably near to the quantile bands width suggesting that the Nhits is providing reliable predictions for the transfer learning procedure.

As it has been proven that the Nhits architecture can make significant predictions of future scenarios using microclimate data collected by sensors in the study area, this neural network can be used to validate future conditions within the clusters. A procedure similar to the second validation approach in the previous experimental validation has been performed. For each cluster, the distribution of the absolute differences of temperature predictions between the cluster center and the cluster sensors has been compared to the one between the cluster center and the sensors located outside the cluster (Fig. 8). The results are consistent with the previous findings; clusters 0, 6, 10 show higher peak for small values of absolute errors and lighter tails for large values of absolute error with respect to the distribution obtained from the sensors outside the cluster (Fig. 8A, C and D). This is also confirmed by the Whitney U statistical test which shows a Pvalue less than 0.05 and so it is possible to reject the null hypothesis that the distribution of the temperature differences inside the cluster is not statistically less than the one outside the cluster. On the contrary, Fig. 8B shows that the distributions of the absolute errors for clusters 2 have a similar shape as confirmed by the Whitney U statistical test which shows a Pvalue higher than 0.05.

These results support the robustness of clustering in reconstructing temperature variations with future predictions. However, it is evident that cluster 0 shows robustness in validating future conditions, in contrast with the previous results obtained during the experimental validation. This might be attributed to the presence of a single sensor that does not fit well within the temperature representation of that cluster. It is plausible that the Nhits may not accurately capture the real variations experienced by this sensor, leading to temporal predictions that are more aligned with those experienced by other sensors. Since the model has been trained using a single source of data common to all sensors, it is likely that the predictions obtained tend to converge towards a similar solution.

4. Conclusions

This paper proposes a computational framework based on machine learning algorithms to optimize a sensors layout according to temperature variations, derived from physical principles, within an open field situated in the Lombardian foothills, Italy. We have experimentally validated that some of the optimized sensors are able to represent the real temperature variations experienced by the study area. We have shown that some of the optimized sensors are also able to represent faithfully

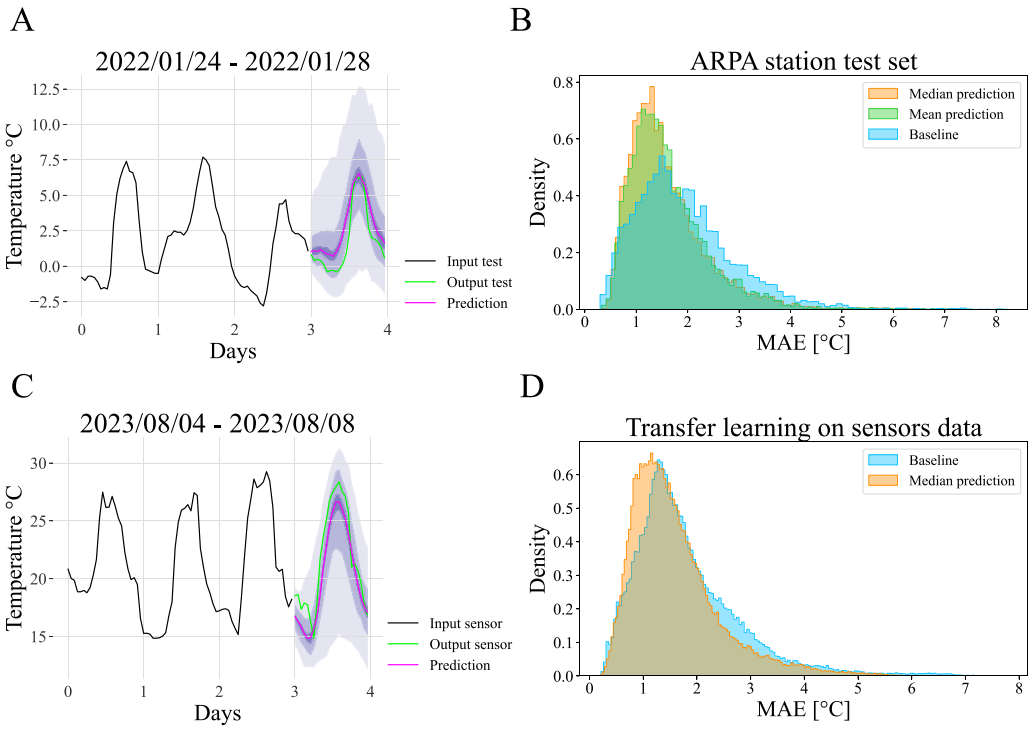

Fig. 7. Nhits results (A) The figure shows an example of the prediction made by the Nhits architecture on the test data from the ARPA station. (B) The figure compares the distribution of the mean absolute error of the prediction by Nhits on the test set for the median prediction, the mean prediction and the baseline prediction. (C) The figure shows an example of the prediction made by the Nhits architecture on the validation clustering data measure from a sensor. (D) The figure compares the distribution of the mean absolute error of the prediction by Nhits on the data measured by the sensors from November 12th, 2022, to June 22nd, 2023, for the median prediction and the baseline prediction.

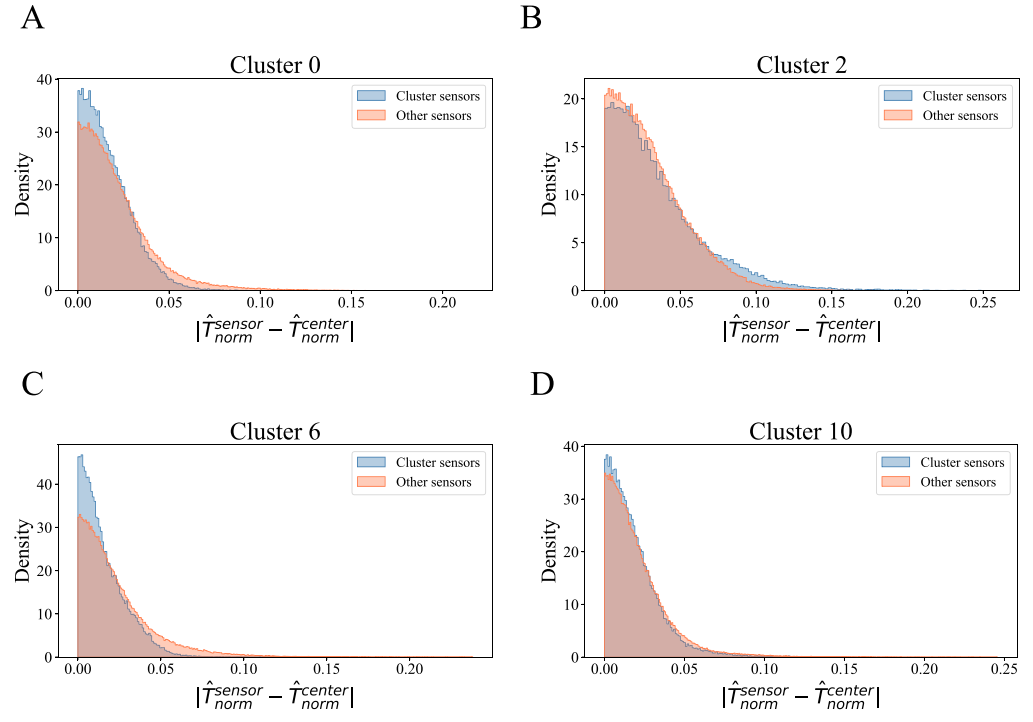

Fig. 8. Validation of Nhits future forecasts. The figures describe the distributions of the median predicted temperature absolute difference between the cluster center and the cluster elements (in blue) and the distribution of the median predicted temperature absolute difference between the center of cluster and all the other elements not in cluster (in red). The figures A, B, C and D describe respectively the data for the validation clusters 0,2,6 and 10.

future temperature scenarios predicted by the Nhits neural network. The representation and prediction of real temperature variations, experienced in an open field which presents complex microclimate pattern, is a difficult task. Nonetheless, the clustering optimization and validation frameworks presented in this paper are able to identify and reconstruct real characteristic temperature patterns.

The main limitations of our approach can be related to the complex task of precisely representing microclimate variations at high resolutions starting from physical principles. The model used in the present paper overlooks local effects generated by the vegetation at the field edges, leading to the identifications of clustering with inconsistent behaviors. Another limitation can be related to the fact that the Nhits neural network has been trained on data which represent the microclimate variations of a single location near to the study area. This can overlook some particular microclimate variations experienced in the study area, which are not present in the training set. This limitation will be addressed in future studies by proposing predictive models trained or fine-tuned for each optimized sensor. These models will forecast the evolution of microclimate with high precision, optimizing precision agriculture management strategies.

Despite these limitations, the current framework has tackled the gaps present in the literature regarding machine learning clustering of microclimate patterns in an open field and the use of deep neural network to validate these emergent patterns. The framework presented here can be applied to any other agricultural field, given the scalability and generality of the computational methods employed. An important development should regard the introduction of new microclimate physical variables in the clustering procedure, providing a more holistic and precise monitoring of the microclimate conditions in the field of precision agriculture.

CRediT authorship contribution statement

Marco Zanchi: Writing – original draft, Visualization, Validation, Software, Methodology, Investigation, Formal analysis, Data curation. **Stefano Zapperi:** Writing – original draft, Supervision, Project administration, Conceptualization. **Caterina A.M. La Porta:** Writing – original draft, Supervision, Project administration, Investigation, Conceptualization.

Declaration of competing interest

The authors declare that they have no known competing financial interests or personal relationships that could have appeared to influence the work reported in this paper.

Data availability

https://github.com/dndg/MicroClimateOptSensorML.

Acknowledgments

The work presented in this paper was made possible in part through the financial support provided by DNDG Srl through the doctoral scholarship of M. Zanchi. CAMLP acknowledges funding from FAIR - Future Artificial Intelligence Research: Adaptive AI methods for Digital Health grant number PNRR_BAC24GVALE_01 PE_0000013, CUP D53C2200238000. We thank DNDG Srl for providing the sensors used in this study, P. Di Nunzio and F. Di Gregorio for assistance in setting up the sensors, and M. Maugeri for useful discussions.

Appendix A. Supplementary data

Supplementary material related to this article can be found online at https://doi.org/10.1016/j.compag.2024.109305.

References

Akhter, R., Sofi, S.A., 2022. Precision agriculture using IoT data analytics and machine learning. J. King Saud Univ.-Comput. Inf. Sci. 34 (8), 5602–5618.

Anastasi, G., Farruggia, O., Re, G.L., Ortolani, M., 2009. Monitoring high-quality wine production using wireless sensor networks. In: 2009 42nd Hawaii International Conference on System Sciences. IEEE, pp. 1–7.

Beck, H.E., Zimmermann, N.E., McVicar, T.R., Vergopolan, N., Berg, A., Wood, E.F., 2018. Present and future Köppen-Geiger climate classification maps at 1-km resolution. Sci. Data 5 (1), 1–12.

Bwambale, E., Abagale, F.K., Anornu, G.K., 2022. Smart irrigation monitoring and control strategies for improving water use efficiency in precision agriculture: A review. Agricult. Water. Manag. 260, 107324.

Challu, C., Olivares, K.G., Oreshkin, B.N., Ramirez, F.G., Canseco, M.M., Dubrawski, A., 2023. Nhits: Neural hierarchical interpolation for time series forecasting. In: Proceedings of the AAAI Conference on Artificial Intelligence. pp. 6989–6997.

Chen, J., Saunders, S.C., Crow, T.R., Naiman, R.J., Brosofske, K.D., Mroz, G.D., Brookshire, B.L., Franklin, J.F., 1999. Microclimate in forest ecosystem and landscape ecology: variations in local climate can be used to monitor and compare the effects of different management regimes. BioScience 49 (4), 288–297.

Cicioğlu, M., Çalhan, A., 2021. Smart agriculture with internet of things in cornfields. Comput. Electr. Eng. 90, 106982.

Comba, L., Biglia, A., Ricauda Aimonino, D., Barge, P., Tortia, C., Gay, P., 2019. Neural network clustering for crops thermal mapping. In: VI International Symposium on Applications of Modelling as an Innovative Technology in the Horticultural Supply Chain Model-IT 1311. pp. 513–520.

Eldar, Y.C., Kutyniok, G., 2012. Compressed Sensing: Theory and Applications. Cambridge University Press.

Escamilla-García, A., Soto-Zarazúa, G.M., Toledano-Ayala, M., Rivas-Araiza, E., Gastélum-Barrios, A., 2020. Applications of artificial neural networks in greenhouse technology and overview for smart agriculture development. Appl. Sci. 10 (11), 3835.

Farooq, M.S., Riaz, S., Abid, A., Umer, T., Zikria, Y.B., 2020. Role of IoT technology in agriculture: A systematic literature review. Electronics 9 (2), 319.

Hartigan, J.A., Wong, M.A., 1979. Algorithm AS 136: A k-means clustering algorithm. J. R. Stat. Soc. Ser. C (Appl. Stat.) 28 (1), 100–108.

Herzen, J., Lässig, F., Piazzetta, S.G., Neuer, T., Tafti, L., Raille, G., Van Pottelbergh, T., Pasieka, M., Skrodzki, A., Huguenin, N., et al., 2022. Darts: User-friendly modern machine learning for time series. J. Mach. Learn. Res. 23 (1), 5442–5447.

Iwasaki, K., Torita, H., Abe, T., Uraike, T., Touze, M., Fukuchi, M., Sato, H., Iijima, T., Imaoka, K., Igawa, H., 2019. Spatial pattern of windbreak effects on maize growth evaluated by an unmanned aerial vehicle in Hokkaido, northern Japan. Agrofor. Syst. 93, 1133–1145.

Jia, Y., Tian, X., Chen, X., Li, X., 2021. An optimization method for the layout of soil humidity sensors based on compressed sensing. J. Sens. 2021, 1–10.

Kamilaris, A., Prenafeta-Boldú, F.X., 2018. Deep learning in agriculture: A survey. Comput. Electron. Agric. 147, 70–90.

Kearney, M.R., Porter, W.P., 2017. NicheMapR–an R package for biophysical modelling: the microclimate model. Ecography 40 (5), 664–674.

Khattab, A., Abdelgawad, A., Yelmarthi, K., 2016. Design and implementation of a cloud-based IoT scheme for precision agriculture. In: 2016 28th International Conference on Microelectronics. ICM, IEEE, pp. 201–204.

Kingma, D.P., Ba, J., 2014. Adam: A method for stochastic optimization. arXiv preprint arXiv:1412.6980.

Maclean, I.M., Mosedale, J.R., Bennie, J.J., 2019. Microclima: An r package for modelling meso-and microclimate. Methods Ecol. Evol. 10 (2), 280–290.

Mann, H.B., Whitney, D.R., 1947. On a test of whether one of two random variables is stochastically larger than the other. Ann. Math. Stat. 50–60.

Oliver, S.T., González-Pérez, A., Guijarro, J.H., 2018. An IoT proposal for monitoring vineyards called SEnviro for agriculture. In: Proceedings of the 8th International Conference on the Internet of Things. pp. 1–4.

Pangga, I.B., Hanan, J., Chakraborty, S., 2011. Pathogen dynamics in a crop canopy and their evolution under changing climate. Plant Pathol. 60 (1), 70–81.

Rodriguez, M.Z., Comin, C.H., Casanova, D., Bruno, O.M., Amancio, D.R., Costa, L.d.F., Rodrigues, F.A., 2019. Clustering algorithms: A comparative approach. PLoS One 14 (1), e0210236.

Rousseeuw, P.J., 1987. Silhouettes: a graphical aid to the interpretation and validation of cluster analysis. J. Comput. Appl. Math. 20, 53–65.

Sai, Z., Fan, Y., Yuliang, T., Lei, X., Yifong, Z., 2016. Optimized algorithm of sensor node deployment for intelligent agricultural monitoring. Comput. Electron. Agric. 127, 76–86.

Sakthipriya, N., 2014. An effective method for crop monitoring using wireless sensor network. Middle-East J. Sci. Res. 20 (9), 1127–1132.

Schultze, S.R., Campbell, M.N., Walley, S., Pfeiffer, K., Wilkins, B., 2021. Exploration of sub-field microclimates and winter temperatures: Implications for precision agriculture. Int. J. Biometeorol. 65, 1043–1052.

Tanny, J., 2013. Microclimate and evapotranspiration of crops covered by agricultural screens: A review. Biosyst. Eng. 114 (1), 26–43.

Uyeh, D.D., Akinsoji, A., Asem-Hiablie, S., Bassey, B.I., Osinuga, A., Mallipeddi, R., Amaizu, M., Ha, Y., Park, T., 2022. An online machine learning-based sensors clustering system for efficient and cost-effective environmental monitoring in controlled environment agriculture. Comput. Electron. Agric. 199, 107139.

Visalini, K., Subathra, B., Srinivasan, S., Palmieri, G., Bekiroglu, K., Thiyaku, S., 2019. Sensor placement algorithm with range constraints for precision agriculture. IEEE Aerosp. Electron. Syst. Mag. 34 (6), 4–15.

Ward, Jr., J.H., 1963. Hierarchical grouping to optimize an objective function. J. Amer. Statist. Assoc. 58 (301), 236–244.

Wen, R., Torkkola, K., Narayanaswamy, B., Madeka, D., 2017. A multi-horizon quantile recurrent forecaster. arXiv preprint arXiv:1711.11053.

Zanchi, M., Zapperi, S., La Porta, C.A., 2023. Harnessing deep learning to forecast local microclimate using global climate data. Sci. Rep. 13 (1), 21062.

Zanchi, M., Zapperi, S., Zanotti, C., Rotiroti, M., Bonomi, T., Gomarasca, S., Bocchi, S., La Porta, C.A., 2022. A pipeline for monitoring water pollution: The example of heavy metals in Lombardy waters. Heliyon 8 (12), e12435.

Zellweger, F., De Frenne, P., Lenoir, J., Rocchini, D., Coomes, D., 2019. Advances in microclimate ecology arising from remote sensing. Trends Ecol. Evol. 34 (4), 327–341.